Iğdır Üniversitesi Fen Bilimleri Enstitüsü Dergisi, 12(3): 1677 - 1689, 2022
Journal of the Institute of Science and Technology, 12(3): 1677 - 1689, 2022

ISSN: 2146-0574, eISSN: 2536-4618

Kimya / *Chemistry* **DOI: 10.21597/jist.1103750**

Araştırma Makalesi / *Research Article*

Geliş tarihi / *Received*: 15.04.2022 **Kabul tarihi / *Accepted*: 20.07.2022**

Atıf İçin: Gören K, Bağlan M, Çakmak İ, 2022. Dietanol Amin Ditiyokarbamat RAFT Ajanının ^{1}H ve ^{13}C NMR Spektrumlarının Teorik İncelenmesi. Iğdır Üniversitesi Fen Bilimleri Enstitüsü Dergisi, 12(3): 1677 - 1689.

To Cite: Gören K, Bağlan M, Çakmak İ, 2022. Theoretical Investigation of ^{1}H and ^{13}C NMR Spectra of Diethanol Amine Dithiocarbamate RAFT Agent. Journal of the Institute of Science and Technology, 12(3): 1677 - 1689.

Dietanol Amin Ditiyokarbamat RAFT Ajanının ^{1}H ve ^{13}C NMR Spektrumlarının Teorik İncelenmesi

Kenan GÖREN[1],Mehmet BAĞLAN[2*], İsmail ÇAKMAK[3]

ÖZET: Bu çalışmada, dietanolamin ditiyokarbamat RAFT bileşiğinin quantum kimyasal çalışmları yapılmıştır. Bu amaçla, bileşik DFT / B3LYP metodunun 6-311G ve B3PW91 metodunun SDD temel seti kullanılarak optimize edildi. GIAO yöntemine göre elde edilen optimize yapı kullanılarak gaz fazında ^{1}H ve ^{13}C NMR kimyasal kayma değerleri hesaplanmıştır. Elde edilen sonuçlara göre teorik verilerin deneysel verilerle uyumlu olduğu görülmüştür. Ayrıca çalışmanın teorik kısmında aynı yöntemler ve temel set kullanılarak sentezlenen bileşiğin FT-IR frekans değerleri deneysel ve teorik olarak karşılaştırılmıştr. Ayrıca molekülerin yapı detayları ve analizi, HOMO ve LUMO enerjileri gibi elektronik özellikler, moleküler elektrostatik potansiyel (MEP) ve termodinamik özellikler gerçekleştirilmiştir. İncelenen molekülün elektrik dipol momenti (μ) ve ilk hiperpolarize edilebilirliği (β), ab initio kuantum mekanik hesaplamalar kullanılarak tahmin edildi. Ayrıca hesaplanan sonuçlar dietanol amin dithiocarbamate (DADC) molekülünün sıfır olmayan değerlerle doğrusal olmayan optik (NLO) davranışa sahip olabileceğini göstermektedir. DADC Mulliken atomik yükleri hesaplandı. Nötral Band Orbital (NBO) analysis DFT / B3PW91/SDD temel seti hesaplanmıştır.

Anahtar Kelimeler: GIAO, DFT, NLO, DADC, ab-initio

Theoretical Investigation of ^{1}H and ^{13}C NMR Spectra of Diethanol Amine Dithiocarbamate RAFT Agent

ABSTRACT: In this study, quantum chemical studies of diethanolamine dithiocarbamate (DADC) RAFT compound were carried out. For this purpose, the composite was optimized by using the DFT / B3LYP method 6-311G and the B3PW91 method SDD basis set. By using the optimized structure obtained according to the GIAO method, ^{1}H and ^{13}C NMR chemical shift values in the gas phase were calculated. According to the results obtained, it was seen that the theoretical data were coherent with the experimental data. In addition, in the theoretical part of the study, the FT-IR frequency values of the compound synthesized by using the same methods and basic set were compared experimentally and theoretically. In addition, the structure details and analysis of molecules, electronic properties such as HOMO and LUMO energies, molecular electrostatic potential (MEP) and thermodynamic properties have been performed. The electric dipole moment (μ) and the initial hyperpolarizability (β) values of the studied molecule were calculated by using ab initio quantum mechanical calculations. In addition, the calculated results show that the (DADC) molecule can have nonlinear optical (NLO) behavior with nonzero values. Neutral Band Orbital (NBO) analysis has been calculated with DFT / B3PW91/SDD basis set.

Keywords: GIAO, DFT, NLO, DADC, ab-initio

[1]Kenan GÖREN (**Orcid ID:** 0000-0001-5068-1762), Kafkas University, Faculty of Arts and Sciences, Department of Organic Chemistry, Kars, Türkiye

[2]Mehmet BAĞLAN (**Orcid ID:** 0000-0002-7089-7111), Kafkas University, Faculty of Arts and Sciences, Department of Organic Chemistry, Kars, Türkiye

[3]İsmail ÇAKMAK (**Orcid ID**:0000-0002-3191-7570), Kafkas University, Faculty of Arts and Sciences, Department of Physical Chemistry, Kars, Türkiye

***Sorumlu Yazar/*Corresponding Author**: Mehmet BAĞLAN, e-mail: mehmetbaglan36@gmail.com

This study was produced from Kenan GÖREN's Master thesis.

INTRODUCTION

The radical polymerization process of a wide variety of monomers can be controlled by using RAFT (Opiyo and Jin 2021; Corrigan et al. 2020). Basically, the RAFT technique can regulate most of the monomers that can be polymerized by radical polymerization(Kartal et al. 2014). The type of monomers used in RAFT polymerization determines the RAFT agent to be used(Yildiko, Ata, and Cakmak 2020). Monomer polymerization can be controlled with dithioesters and trithiocarbonates(Baglan et al. 2018). In molecular chemistry, many properties such as band structure and bond energy calculation of solids can be determined by using density functional theory (DFT), which is one of the most successful theories in finding properties of matter(Yildiko et al. 2021).

Calculations made using DFT can be used to support experimental studies as well as to pioneer studies that have not been done experimentally (Obot, Macdonald, and Gasem 2015; Janeoo et al. 2022). While a compound has not been synthesized yet, many of its properties can lead to experimental studies and engineering studies by calculating theoretically whether it is structurally stable or not(Sherin and Manojkumar 2020; Lohith et al. 2022). Another advantage of density functional theory calculations is that it makes it easier to carry out costly studies and also allows research under extraordinary conditions such as high pressure(Nageswari et al. 2018; Sucheta et al. 2022). Nowadays, the density functional theory (DFT) method is broadly utilized to supply data around the electronic and geometric structure of molecules(Shukla and Yadava 2022; Jin et al. 2022). The vital feature of polymer DFT is its chain configuration, which is not considered in other DFTs, illuminating the free energy function of the polymer DFT is an important issue in the appropriate relationship between the cross-section density profile and the overall potential(Zahedi and Farzi 2022; Rahman et al. 2022). With this strategy, the structural properties of the particles, dipole moment, etc. computable.

In this study, the theoretical spectroscopic properties of the DADC molecule have been examined by using the DFT / B3LYP / 6-311G and B3PW91/SDD basis sets and have been compared with the experimentally found values (Sert et al. 2020; Tarchouna, Chaabane, and Rahaiem 2016).

MATERIALS AND METHODS

Calculation Methods

In this study, the Gaussian 09W package program, which is a computer-aided computing program with a wide variety of basic set options such as ab-initio, molecular mechanics and quasi-experimental methods, was used. DFT methods are widely used in GIAO NMR methods. There are similarities with the starting methods. It has some computational advantages over NMR such as DFT/B3LYP/6-311G and B3PW91/SDD.

RESULTS AND DISCUSSION

^{1}H NMR Spectrum

In this study, experimental values of DADC ^{1}H and ^{13}C NMR spectra have been compared by examining their theoretical spectroscopic properties. After the DADC structure was minimized with the Gaussian 09W program and the DFT / B3LYP / 6-311G and B3PW91/SDD method, ^{1}H shift values were calculated according to the GIAO method(Fizer et al. 2021; Gancheff and Denis 2015). MS has been taken as reference in the calculations. The calculated ^{1}H values have been compared with the experimental data as shown in Table 1 and figure 1. It has been observed that there is a correlation between experimental data and theoretical data as Yexperimental= 0.92 Xtheoretical+0.78. Here, the correlation coefficient R=0.966 shows a good coherence.

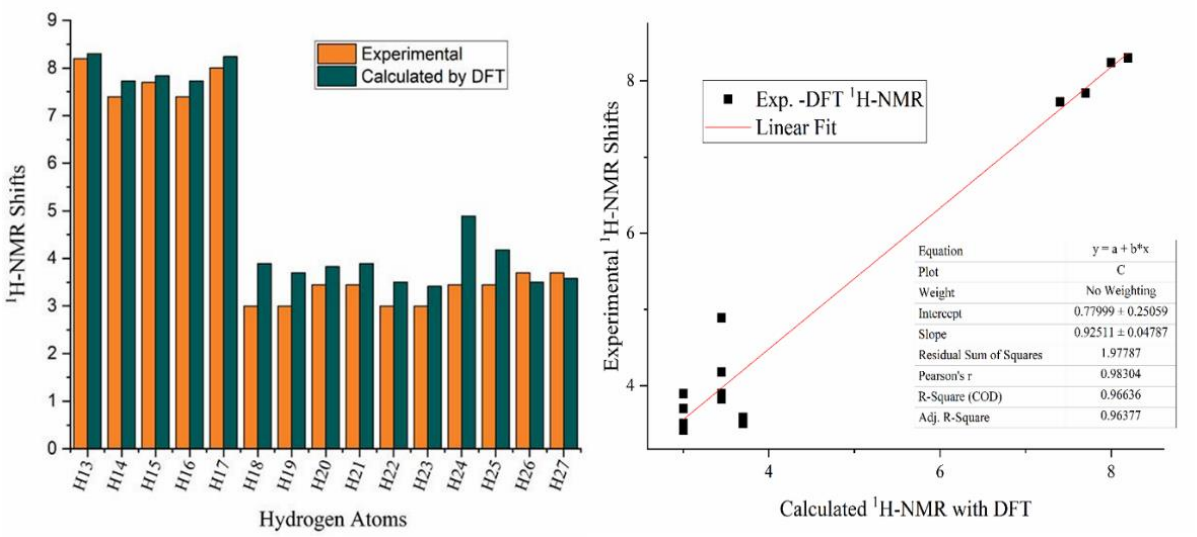

Figure 1. Comparison of DADC ^{1}H NMR experimental and DFT theoretical values

Table 1. DADC ^{1}H NMR Experimental and Theoretical Values

Hydrogen No	Experimental	B3LYP/6-31G8(dp)/DFT	Difference
$_{13}H$	8.20	8.30	-0.1
$_{14}H$	7.40	7.73	-0.33
$_{15}H$	7.70	7.84	-0.14
$_{16}H$	7.40	7.73	-0.33
$_{17}H$	8.00	8.24	-0.24
$_{18}H$	3.00	3.90	0.90
$_{19}H$	3.00	3.70	-0.70
$_{20}H$	3.45	3.83	-0.38
$_{21}H$	3.45	3.89	0.44
$_{22}H$	3.00	3.51	-0.51
$_{23}H$	3.00	3.41	0.41
$_{24}H$	3.45	4.90	-1.44
$_{25}H$	3.45	4.18	-0.73
$_{26}H$	3.7	3.51	0.19
$_{27}H$	3.7	3.58	0.12

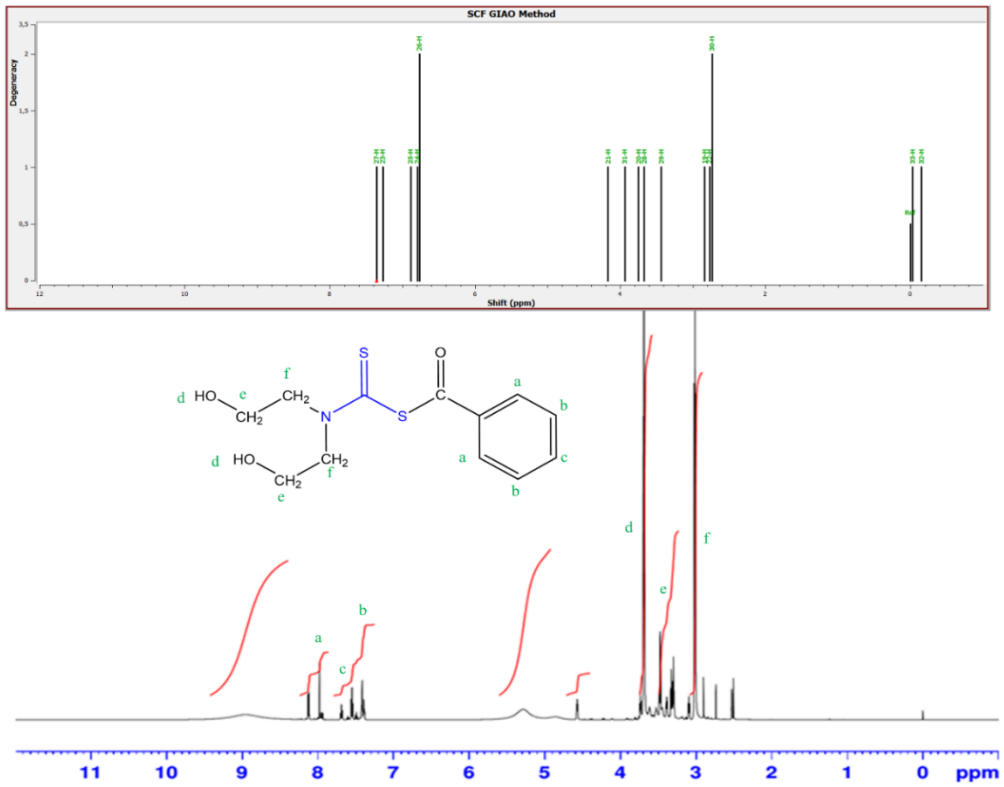

Figure 2. DADC RAFT Ajanı ^{1}H NMR Spektrumu ve Theoretical DFT with TMS B3LYP/6-311G GIAO

The studied molecule also has eight hydrogen atoms (ring, OH and CH_2 group). Experimental ^{1}H NMR is seen at 8.07 for a, 7.7 for c, 7.5 for b, 3.7 for d, 3.5 for e, 3.0 ppm for f. All predicted chemical shift values are in good coherence with the experimental values.

Theoretical Calculation of ^{13}C NMR Spectra

After the DADC structure was minimized with the Gaussian 09W program and the DFT/B3LYP/6-311G and B3PW91/SDD methods, the ^{13}C shift values were calculated according to the GIAO method(Onchoke 2021). TMS was taken as reference in the calculations. The calculated ^{13}C values were compared with the experimental data as shown in Table 2 and Figure 2. It has been observed that there is a relationship such as Yexperimental= 0.95 Xtheoretical + 19.17. while Here,the slope should be 0.95, it has been seen that the values were compatible with each other.

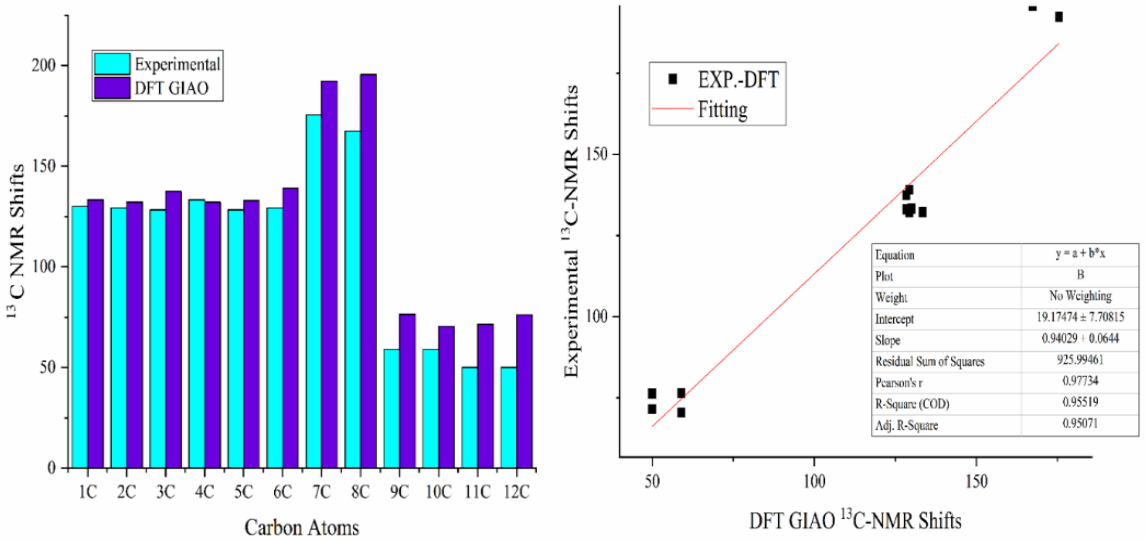

Figure 3. Comparison of DADC experimental and DFT GIAO ^{13}C NMR shift values

Table 2. Experimental and theoretical ^{13}C NMR DFT/B3LYP/6-311G chemical shift values (ppm) of DADC according to TMS

Carbon No	Experimental	B3LYP/6-31G(dp)/DFT	Difference
$_{1}C$	130.00	133.29	-3.29
$_{2}C$	129.31	132.23	-2.92
$_{3}C$	128.40	137.42	-9.02
$_{4}C$	133.40	132.23	1.17
$_{5}C$	128.40	133.02	-4.62
$_{6}C$	129.31	139.10	-9.79
$_{7}C$	175.50	192.29	-16.79
$_{8}C$	167.40	195.59	-28.19
$_{9}C$	59.00	76.42	-17.46
$_{10}C$	59.00	70.46	-11.46
$_{11}C$	50.00	71.49	-21.49
$_{12}C$	50.00	76.28	-26.28

There are eight carbon atoms in the DADC molecule (ring). The result in Table 3 appears that the extent of carbon ^{13}C NMR chemical shifts of the normal natural molecule is for the most part > 100 ppm. In this study, aromatic carbons between 125 and 135 ppm have been observed in the carbon 13C NMR spectrum for the DADC molecule. The high electronegative nature of the oxygen (O) and nitrogen (N) atoms polarizes the electron distribution in the bond of the DADC molecule to the adjacent carbon atom, reducing the electron density in the bridge for the cap molecule. Therefore, the chemical shift value appears to be moderately high for the DMSO-d6 solvent cap molecule under investigation at 172 and 162 ppm (C(a), C(b)). The calculated ^{13}C NMR chemical shift values are in good coherence with the experimental values.

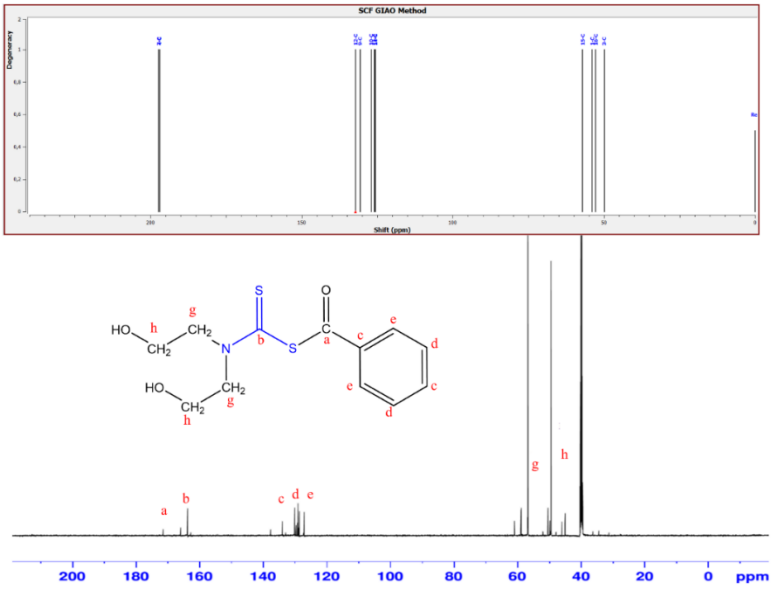

Figure 4. DADC ^{13}C NMR Spektrumu ve Theoretical with TMS B3LYP/6-311G GIAO

FT-IR spectroscopy

The experimental IR values of the DADC molecule are in the range of OH, 3307, ArC-H, 2834 C=O, 1720, C=S, 1649, C-N, 1060, with little difference between theoretical values. This is because it is in the gas phase.

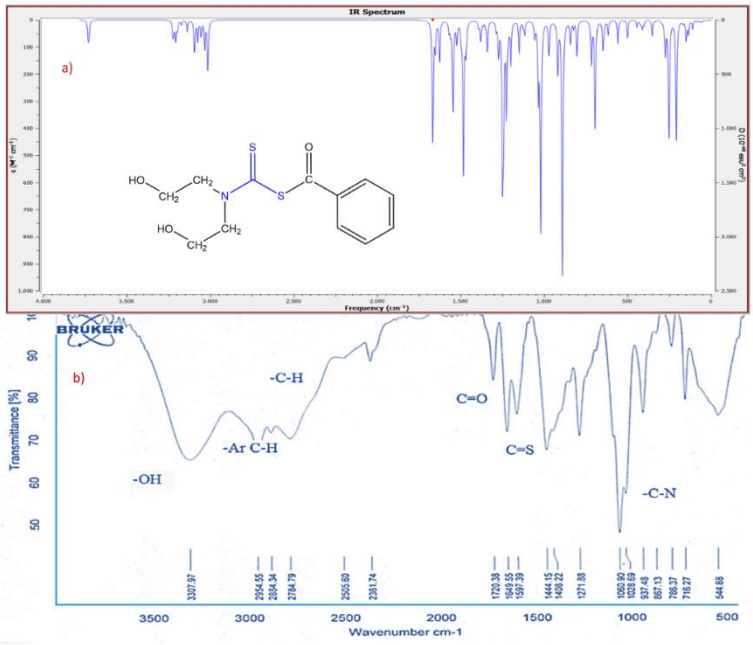

Figure 5. Theoretical DFT FT IR Spectrum of DADC Compound

Structure Details and Analysis

Optimized structural parameters calculated with the DFT/B3LYP/6-311G and B3PW91/SDD basis set(Solğun et al. 2020; Cabir et al. 2020). The optimized molecular, bond lengths and bond angles between particles were compared with each other utilizing the two strategies are listed in Table 3. When the two methods were compared, the bond lengths of S-C atoms in the DADC nuclei have been calculated as 1.89 Å in B3LYP/6-311G and 1.69 Å in B3PW91/SDD. It has been observed that the bond

lengths were shorter in the second method. In aromatic and aliphatic structures, bond lengths are congruous with both strategies. The slight differences between them are due to the affectability of the strategies. Both methods are compatible.

Table 3. Theoretically obtained some bond lengths (Å) and bond angles (º) of the molecule

Bond Lengths	B3LYP/6-311G	B3PW91/SDD	Bond Lengths	B3LYP/6-311G	B3PW91/SDD
S6-C4	1.89	1.88	C14-H27	1.08	1.09
S5-C4	1.71	1.69	C12-H25	1.09	1.09
N2-C1	1.48	1.48	C10-H23	1.09	1.09
N2-C4	1.49	1.36	C16-H30	1.10	1.10
S6-C7	1.88	1.86	C15-H28	1.10	1.10
C7-C9	1.49	1.49	C3-H21	1.09	1.09
C1-C15	1.54	1.53	C1-H19	1.10	1.10
C3-C16	1.54	1.53	C7-O8	1.24	1.24
C9-C14	1.42	1.41	C15-O17	1.46	1.46
C9-C10	1.41	1.41	C16-O18	1.46	1.46
Bond Angles	**B3LYP/6-311G**	**B3PW91/SDD**	**Bond Angles**	**B3LYP/6-311G**	**B3PW91/SDD**
C9-C7-S6	114.98	114.58	H20-C1-N2	110.10	109.91
C7-C9-C14	117.23	117.25	C3-N2-C4	118.98	118.72
C7-C9-C10	123.17	123.10	C3-C16-018	104.60	104.76
S6-C7-O8	121.23	121.45	N2-C3-C16	113.11	113.18
C9-C7-O8	123.78	123.97	H28-C15-H29	109.75	109.50
Bond Angles	**B3LYP/6-311G**	**B3PW91/SDD**	**Bond Angles**	**B3LYP/6-311G**	**B3PW91/SDD**
C11-C10-C9-C7	-179.81	-179.83	H20-C1-N2-C3	170.58	170.70
C10-C9-C7-O8	-170.62	-170.04	C4-N2-C1-C15	116.70	116.87
C1-C15-O17- H32	175.62	176.20	C3-C16-O18-H33	-157.99	-158.05

HOMO and LUMO Analysis

The fundamental electronic parameters related to orbitals in a particle are the most elevated and possessed atomic orbital (HOMO) and the least abandoned atomic orbital (LUMO) and their energy gap (Janeoo et al. 2022). HOMO are electrons within the furthest (most noteworthy vitality) orbital that can act as an electron donor (Ağırtaş et al. 2020). The LUMO is the deepest (least vitality) orbital that has sufficient space to acknowledge electrons and can act as an electron acceptor (Solğun, Yıldıko, and Ağırtaş 2021).

In addition to these, E_{LUMO} and E_{HOMO} graphics have been also taken. E_{HOMO} = -5.78 eV for the DFT/B3LYP/6-311G method of the molecule, E_{HOMO} = -5.87 eV for the DFT/ B3PW91/SDD method, E_{LUMO} = -2.30 eV for the B3PW91/SDD method have been calculated as E_{LUMO} = -2.32 eV values. For other orbitals; E_{HOMO} = -6.34 eV for the DFT/B3LYP/6-311G method, E_{HOMO} = -6.44 eV for the B3PW91/SDD method, and E_{LUMO} = -1.54 eV for the DFT/B3LYP/6-311G method, E_{LUMO} = -1.53 eV for the B3PW91/SDD method The eV value has been calculated.

Table 4. Comparison of HOMO, LUMO and chemical reactivity descriptors by DFT/B3LYP/6-311G-DFT/ B3PW91/SDD levels methods at 298.15 K in ground state

Molecules Energy	DFT/B3LYP/6-311G	DFT/ B3PW91/SDD
E_{LUMO}	-2.30	-2.32
E_{HOMO}	-5.78	-5.87
E_{LUMO+1}	-1.54	-1.53
E_{HOMO-1}	-6.34	-6.44
Energy Gap (Δ)$\lvert E_{HOMO}- E_{LUMO}\rvert$	3.48	3.55
Electron Affinity ($A = -E_{LUMO}$)	2.30	2.32
Ionization Potential ($I = -E_{HOMO}$)	5.78	5.87
Chemical Potential (μ) = ($E_{HOMO}+E_{LUMO}$) /2	-4.04	-4.09
Electronegativity (χ)= - ($E_{HOMO}+E_{LUMO}$) /2	4.04	4.09
Chemical hardness (η)= ($E_{HOMO}-E_{LUMO}$)/2)	1.74	1.77
Global softness ($s = 1/2\ \eta$)	0.29	0.28
Global electrophilicity ($\omega= \mu^2/2\ \eta$)	4.69	4.72

The calculated comes about and their comparison with the two strategies have been displayed in Table 4. LUMO and HOMO plots of the DADC compound has been also taken. Figures 7, 8, The HOMO and LUMO orbitals show how the particle interacts between atoms with other species. It also to aids

distinguish to recognize band gap, chemical reactivity and active stability. This is due to the computational accuracy from different parameters of these two methods.

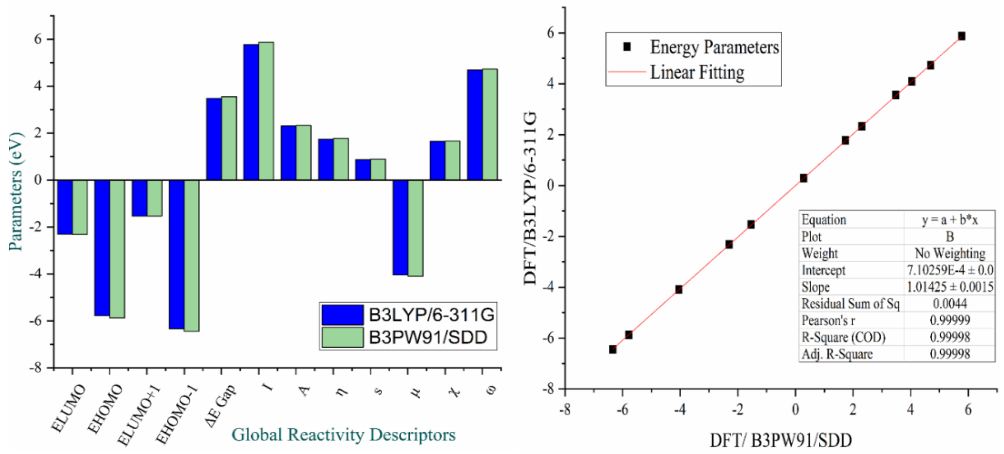

Figure 6. Comparison of parameters and chemical reactivity descriptors and correlation graphs between DFT / B3LYP/ 6-311G and DFT/ B3PW91/SDD methods

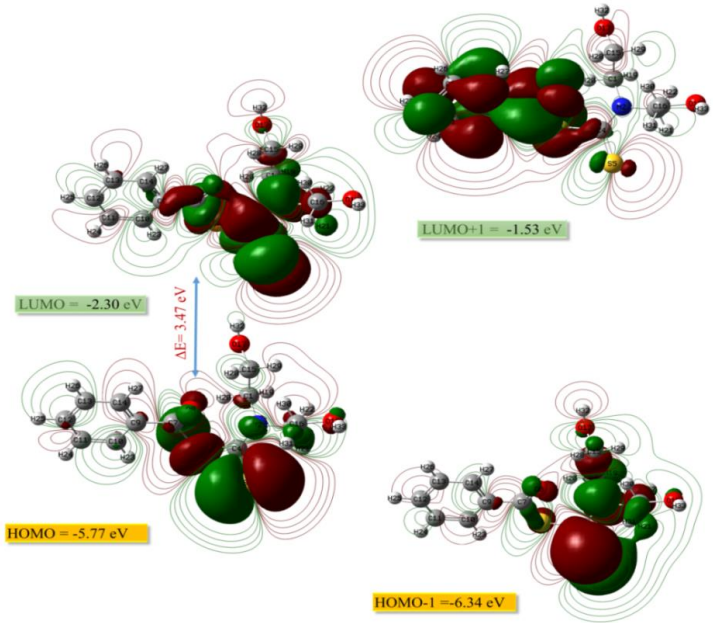

Figure 7. Boundary molecular orbitals of DADC compound according to DFT/B3LYP/6-311G level

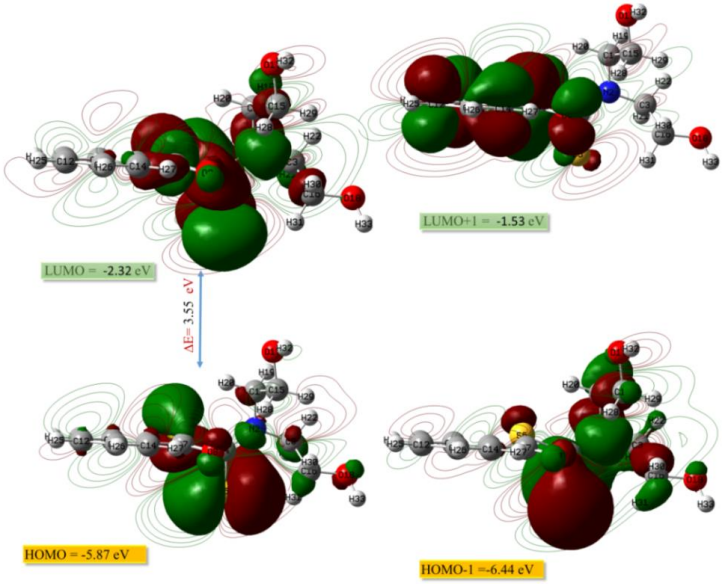

Figure 8. Boundary molecular orbitals of DADC compound according to DFT/B3PW91/SDD level

Non-Linear Optical Properties (NLO)

The first derivative of an important attribute, the dipole moment, is defined as the energy associated with an applied electric field in a molecule, fundamentally etc. Van der Waals type dipole dipole forces are used to analyze intermolecular interactions; the bigger the dipole moment, the stronger the intermolecular attraction(Akman et al. 2020). The dipole moment, molecular polarization and hyperpolarizability values are important in determining the Nonlinear Optical (NLO) properties. Parameters for the DFT/B3LYP/6-311G method were determined as $\mu = 4.73$ D, $\alpha = 720.93$ au, $\beta = 1.087 \times 10^{-28}$ esu and for the B3PW91/SDD method $\mu = 4.77$ D, $\alpha = 724.83$ au, $\beta = 1.074 \times 10^{-28}$ esu in the gas phase. These results for the molecule under investigation imply that these are NLO materials.

Table 5. DFT/B3LYP- B3PW91 belong to 6-311G and SDD basis set calculated dipole moments (Debye), (au) polarizability, β components, and β tot Zn-Pc value.

Parameters	B3LYP/6-311G	B3PW91/SDD	Parameters	B3LYP/6-311G	B3PW91/SDD
μ_x	-2.73	-2.74	β_{XXX}	-129.09	-133.92
μ_y	3.45	3.46	β_{XXY}	-2.53	-0.12
μ_z	1.73	1.82	β_{XYY}	5.04	4.36
$\mu_{(D)}$	4.73	4.77	β_{YYY}	80.35	87.70
α_{xx}	-99.79	-100.35	β_{XXZ}	37.71	39.34
α_{yy}	-123.55	-124.02	β_{XYZ}	-20.86	-21.81
α_{zz}	-116.35	-117.26	β_{YYZ}	26.01	27.07
α_{XY}	3.42	3.48	β_{XZZ}	44.01	43.38
α_{XZ}	5.48	5.62	β_{YZZ}	-7.37	-4.62
α_{YZ}	7.30	7.44	β_{ZZZ}	27.44	30.33
α (au)	720.93	724.83	β (esu)	1.087×10^{-28}	1.074×10^{-28}

Mulliken Atomic Charges (B3LYP/6-311G- B3PW91/SDD)

Mulliken atom charges the atom for the DADC compound calculated with the PM6 set of the B3LYP/6-311G - B3PW91/SDD method (Dwivedi and Kumar 2021). Data obtained from Mulliken load distribution are presented in Figure 9 and Table 6. The Mulliken charge distribution shows that the amine group nitrogen atom is N2(-0.03) by the B3LYP/6-311G method and N2(0.01) by the B3PW91/SDD method for the SM method. These have been calculated as C1(- 0.34) with B3LYP/6-311G method, C1(-0.35) with B3PW91/SDD method, C9(0.38) with B3LYP/6-311G method, C9(0.39) with B3PW91/SDD method.

Table 6. Mulliken atomic charges calculated for by DFT / B3LYP and B3PW91 methods with 6-311G and SDD base set.

	B3LYP/6-311G	B3PW91/SDD		B3LYP/6-311G	B3PW91/SDD
C1	-0.34	-0.35	O17	-0.48	-0.51
N2	-0.03	0.01	O18	-0.47	-0.51
C3	-0.36	-0.35	H19	0.22	0.25
C4	-0.49	-0.53	H20	0.26	0.26
S5	0.16	0.05	H21	0.28	0.27
S6	0.23	0.17	H22	0.23	0.24
C7	-0.17	-0.15	H23	0.25	0.25
C8	-0.19	-0.23	H24	0.23	0.23
C9	0.38	0.39	H25	0.23	0.23
C10	-0.28	-0.30	H26	0.23	0.23
C11	-0.22	-0.23	H27	0.28	0.26
C12	-0.22	-0.21	H28	0.21	0.25
C13	-0.22	-0.22	H29	0.20	0.20
C14	-0.37	-0.33	H30	0.20	0.23
C15	-0.33	-0.28	H31	0.21	0.23
C16	-0.32	-0.27	H32	0.35	0.37

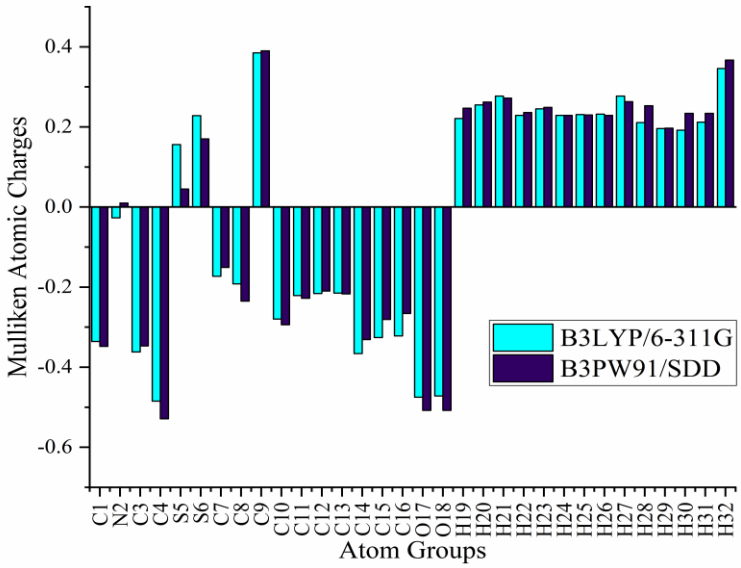

Figure 9. Mulliken population analysis chart of DADC compound by DFT / B3LYP and DFT/B3PW91 methods with 6-311G and SDD base set.

The calculated Mulliken atomic charges have an vital part within the application of quantum chemical computation on the atomic system, since atomic charges influence dipole moment, molecular polarization, electronic structure, and numerous properties of molecular systems. The charge dissemination on the particle demonstrates the arrangement of the giver and acceptor pair, including charge exchange within the particle. Mulliken charge particle was calculated for the DFT / B3LYP / 6-311G and B3PW91/SDD basis set. It was observed that a few C atoms were positive and of a few were negative.

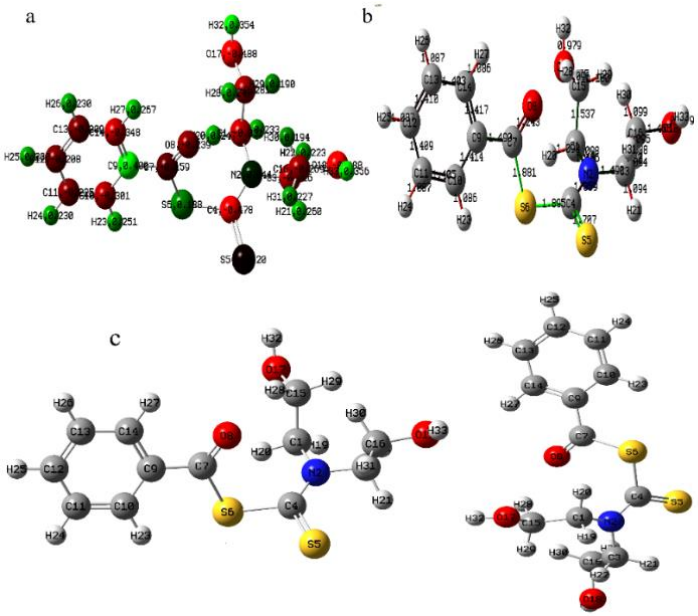

Figure 10. DADC molecule with B3LYP/6-311G set a) mulliken b) bond length c) structure optimization

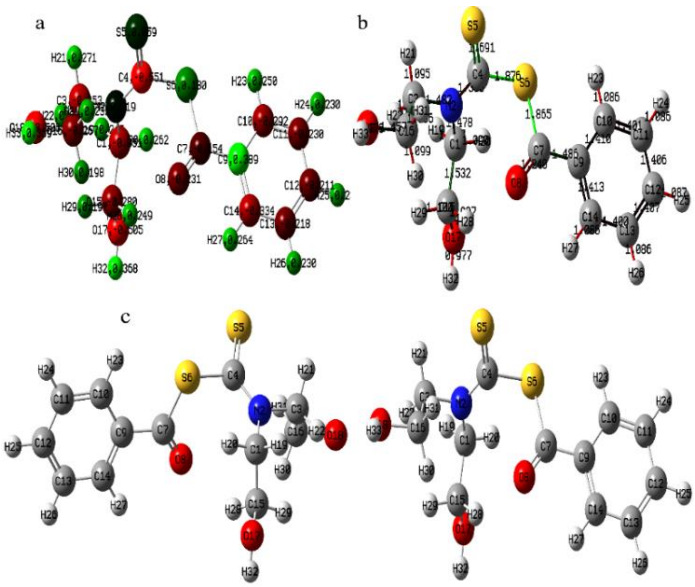

Figure 11. DADC molecule with B3PW91/SDD set a) mulliken b) bond length c) structure optimization

Molecular electrostatic potential (MEP)

In our study, to discover reactive regions of electrophilic or nucleophilic assalts of the DADC molecule we are considering, With the DFT/B3LYP/6-311G and B3PW91/SDD set, the optimized geometry was calculated by MEP (Altun et al. 2021). In Figure 12, regions with negative (red) electrostatic potential values on the MEP surface indicate electrophilic reactivity, while positive (blue) regions indicate nucleophilic reactivity and neutral (green) electrostatic potential regions.

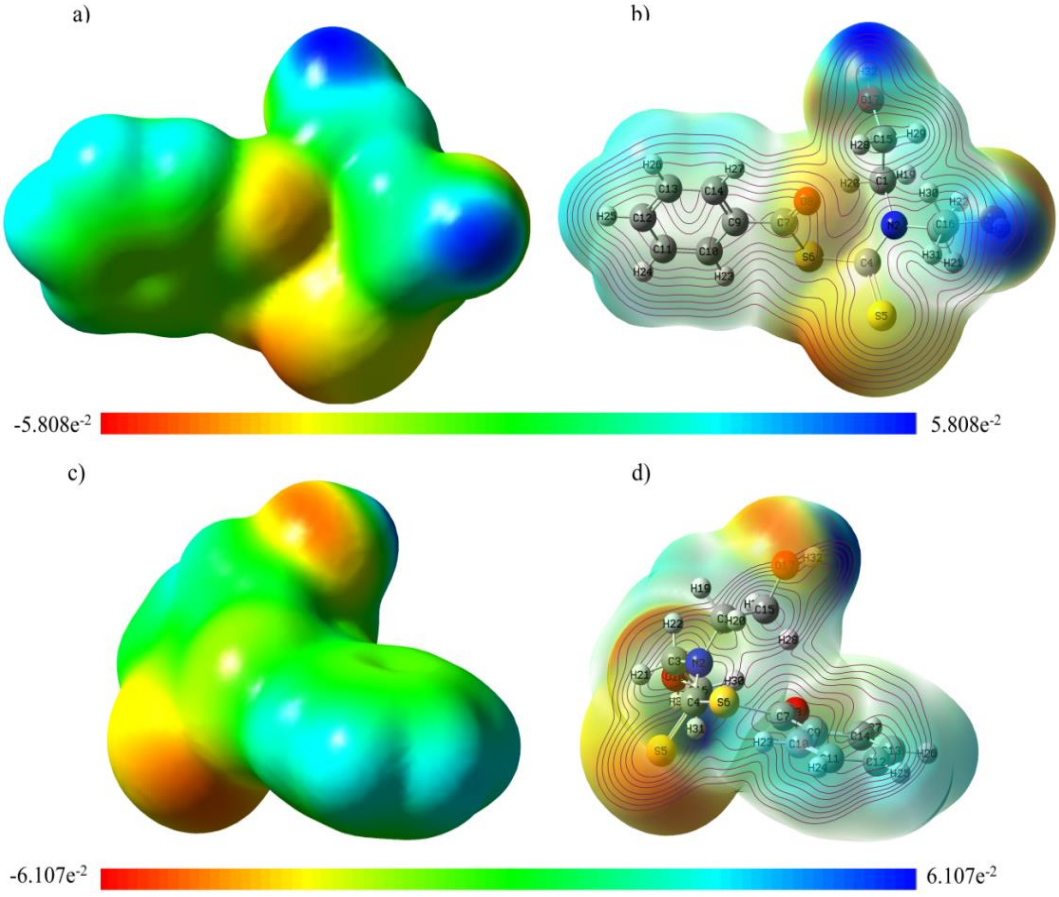

Figure 12. Molecular electrostatic potential surface by DFT / B3LYP and B3PW91 methods with 6-311G and SDD basis set

NBO Analysis

In the NBO analysis, the donor-recipient interactions were concluded with the second-order Fock matrix method. The interaction between occupancy losses from an idealized Lewis structure to an empty non-Lewis orbital is due to second-order distortion (Isravel et al. 2021). The following equation related to the stabilization energy E(2), donor (i) and acceptor (j), i and j delocalization terms has been benefited from the following equation.

$$E(2) = \Delta Eij = qi \frac{(Ei,j)^{2}}{(Ej-Ei)} \quad (1)$$

Ei and Ej are diagonal elements, qi is donor orbital occupancy, and Fi,j are non-diagonal NBO Fock matrix elements. The bigger the E(2) esteem, the more strongly the interaction between electron givers and electron acceptors, that's the more prominent the propensity to give from electron from the transmitters to electron acceptors and the more noteworthy the conjugation of the whole system. To explain the conjugation, hyperconjugation and delocalization of electron thickness inside the particle (Buvaneswari et al. 2021), NBO investigation has been performed on the particle at the DFT/B3PW91/SDD level. The intramolecular hyperconjugative interaction of the distribution to σ (C7-O8) σ electrons in the ring causes stabilization of a portion of the ring, as clearly seen in Table 7. The intramolecular hyperconjugative interaction of the σ* (C4-S5) and anti σ* (C15-H29) bond on the ring causes a stabilization of 280.64-91.26 kcal/mol. These values increased conjugation resulting in strong localization.

Table 7. Selected NBO results to show the formation of Lewis and non-Lewis orbitals for DADC using the DFT/B3PW91/SDD theory level

NBO(i)	Type	ED/e	NBO(j)	Type	ED//e	E(2)[a] (Kcal/mol)	E (j)-E(i)[b] (a.u.)	F (i, j)[c] (a.u)
C1-N2	σ	1.97402	C4-S5	π*	0.14643	4.03	1.15	0.063
C1-N2	σ	1.97402	C15-O17	σ*	0.01954	2.07	0.98	0.040
C1-C15	σ	1.97916	N2-C4	σ*	0.10052	4.22	0.89	0.056
C1-H20	σ	1.97625	N2-C3	σ*	0.02242	4.31	0.83	0.053
N2-C3	σ	1.97125	C4-S6	σ*	0.10813	4.86	1.00	0.063
N2-C3	σ	1.97125	C16-O18	σ*	0.02010	2.03	0.99	0.040
C7-C9	σ	1.97645	C13-C14	σ*	0.02080	4.28	1.05	0.060
C9-C14	π	1.75613	C7-O8	π *	0.24610	21.40	0.23	0.063
C9-C14	π	1.75613	C10-C11	π*	0.16355	11.46	0.31	0.055
C9-C14	π	1.75613	C12-C13	π*	0.17040	10.12	0.31	0.051
C10-C11	π	1.80955	C9-C14	π*	0.21564	11.89	0.31	0.055
C10-C11	π	1.80955	C12-C13	π*	0.17040	11.88	0.31	0.054
C15-H29	σ	1.87789	C16-H30	σ*	0.12335	90.02	1.25	0.299
C16-H30	σ	1.87696	C15-H29	σ*	0.12473	91.26	1.25	0.301
C16-H30	σ	1.87696	C16-H30	σ*	0.12335	5.92	1.25	0.077
C16-H30	σ	1.87696	C15-O17	σ*	0.01954	5.40	0.76	0.059
N2-C4	σ	1.97914	C1-N2	σ*	0.02460	6.24	0.01	0.031
N2-C4	σ	1.97914	N2-C3	σ*	0.02242	5.69	0.02	0.035
C4-S5	σ	1.97781	N2-C3	σ*	0.02242	32.19	0.02	0.058
C4-S5	σ	1.97781	C4-S5	σ*	0.21690	280.64	0.15	0.429

CONCLUSION

The main subject of our study is the comparison of experimental and theoretical spectroscopic values of molecular modeling of DADC. As it is known, the purpose of computational chemistry programs is to clarify the properties of molecules with the help of computers without the need for experiments. To determine the molecular structure and spectroscopic values of the RAFT agent we synthesized, the Gaussian 09W program was calculated with the 6-311G and SDD base set using the density functional method (DFT/B3LYP/B3PW91). NMR spectroscopy has been successfully and widely used in molecular structure elucidation. The results of the experimental studies are controlled by ^{1}H-NMR and ^{13}C-NMR spectroscopic techniques, which are the NMR spectrum series. NMR and ^{13}C-NMR spectroscopic values obtained by theoretical calculations with the experimental data of the DADC.

As a result, the obtained data showed the reliability of the method used. In this study, the harmony in the comparison of the experimental theoretical information obtained about the structure and chemical properties of DADC, which was synthesized for use in controlled radical polymerization, has been followed.

Conflict of Interest

The article authors declare that there is no conflict of interest between them.

Author's Contributions

The authors declare that they have contributed equally to the article.

REFERENCES

Ağırtaş, Mehmet Salih, Derya Güngördü Solğun, Ümit Yildiko, and Abdullah Özkartal. 2020. 'Design of novel substituted phthalocyanines; synthesis and fluorescence, DFT, photovoltaic properties', *Turkish journal of chemistry*, 44: 1574-86.

Akman, Murat, Ahmet Cagri Ata, Umit Yildiko, and İsmail Çakmak. 2020. 'Molecular structure, frontier molecular orbitals, NBO, MESP and thermodynamic properties of 5,12-dibromo perylene with DFT calculation methods', *International Journal of Chemistry and Technology*, 4: 49-59.

Altun, Kenan , Ümit Yildiko, Aslihan Aycan Tanriverdi, and Ismail Cakmak. 2021. 'Structural and spectral properties of 4-(4-(1-(4-Hydroxyphenyl)-1-phenylethyl)phenoxy)phthalonitrile: Analysis by TD-DFT method, ADME analysis and docking studies', *International Journal of Chemistry and Technology*, 2: 147-55.

Baglan, Mehmet, Ümit Yildiko, İsmail Çakmak, and Ahmet Turan Tekeş. 2018. 'Synthesis of PMMA-b-PEG-b- PMMA by controlled Polymerization Using Macro-RAFT Agents', *Journal of the Institute of Science and Technology*, 8: 243-54.

Buvaneswari, M., R. Santhakumari, C. Usha, R. Jayasree, and Suresh Sagadevan. 2021. 'Synthesis, growth, structural, spectroscopic, optical, thermal, DFT, HOMO–LUMO, MEP, NBO analysis and thermodynamic properties of vanillin isonicotinic hydrazide single crystal', *Journal of Molecular Structure*, 1243: 130856.

Cabir, Beyza, Umit Yildiko, Mehmet Salih Ağırtaş, and Sabit Horoz. 2020. 'Computational DFT calculations, photovoltaic properties and synthesis of (2R, 3S)-2, 3, 4-trihydroxybutoxy substituted phthalocyanines', *Inorganic and Nano-Metal Chemistry*, 50: 816-27.

Corrigan, Nathaniel, Kenward Jung, Graeme Moad, Craig J. Hawker, Krzysztof Matyjaszewski, and Cyrille Boyer. 2020. 'Reversible-deactivation radical polymerization (Controlled/living radical polymerization): From discovery to materials design and applications', *Progress in Polymer Science*, 111: 101311.

Dwivedi, Apoorva, and Abhishek Kumar. 2021. 'Molecular Docking and Comparative Vibrational Spectroscopic Analysis, HOMO-LUMO, Polarizabilities, and Hyperpolarizabilities of N-(4-Bromophenyl)-4-Nitrobenzamide by Different DFT (B3LYP, B3PW91, and MPW1PW91) Methods', *Polycyclic Aromatic Compounds*, 41: 387-99.

Fizer, Maksym, Mikhailo Slivka, Nataliya Korol, and Oksana Fizer. 2021. 'Identifying and explaining the regioselectivity of alkylation of 1,2,4-triazole-3-thiones using NMR, GIAO and DFT methods', *Journal of Molecular Structure*, 1223: 128973.

Gancheff, Jorge S., and Pablo A. Denis. 2015. 'Relative affinity of bambus[6]uril towards halide ions: A DFT/GIAO approach in the gas phase, and in the presence of the solvent employing discrete and discrete-continuum models', *Computational and Theoretical Chemistry*, 1064: 35-44.

Isravel, Antony Danish, Jebasingh Kores Jeyaraj, Sasitha Thangasamy, and Winfred Jebaraj John. 2021. 'DFT, NBO, HOMO-LUMO, NCI, stability, Fukui function and hole – Electron analyses of tolcapone', *Computational and Theoretical Chemistry*, 1202: 113296.

Janeoo, Shashi, Reenu, Amandeep Saroa, Rakesh Kumar, and Harminder Kaur. 2022. 'Computational investigation of bioactive 2,3-diaryl quinolines using DFT method: FT- IR, NMR spectra, NBO, NLO, HOMO-LUMO transitions, and quantum-chemical properties', *Journal of Molecular Structure*, 1253: 132285.

Jin, Huixin, Jianxin Zhang, Wenyang Zhang, Youjian Zhang, Shiyu Ma, Yiqun Du, Jingyu Qin, and Qi Wang. 2022. 'Experimental studies and DFT calculations to predict atomic arrangements at twin boundaries and distribution behaviors of different solutes in complex intermetallics', *Journal of Physics and Chemistry of Solids*, 161: 110453.

Kartal, Baris, Umit Yildiko, Soner Ozturk, Ahmet C. Ata, and Ismail Cakmak. 2014. 'Study of Solution Polymerization of Styrene in the Presence of Poly(ethylene glycol)-RAFT Agents Possessing Benzoyl Xanthate Derivatives', *Journal of Macromolecular Science, Part A*, 51: 990-98.

Lohith, T. N., S. Shamanth, M. A. Sridhar, K. Mantelingu, and N. K. Lokanath. 2022. 'Synthesis, molecular structure, Hirshfeld surface, energy framework and DFT studies of 1,3,4 oxadiazole derivative', *Journal of Molecular Structure*, 1252: 132203.

Nageswari, G., Gene George, S. Ramalingam, and M. Govindarajan. 2018. 'Electronic and vibrational spectroscopic (FT-IR and FT-Raman) investigation using ab initio (HF) and DFT (B3LYP and B3PW91) and HOMO/LUMO/MEP analysis on the structure of l-serine methyl ester hydrogen chloride', *Journal of Molecular Structure*, 1166: 422-41.

Obot, I. B., D. D. Macdonald, and Z. M. Gasem. 2015. 'Density functional theory (DFT) as a powerful tool for designing new organic corrosion inhibitors. Part 1: An overview', *Corrosion Science*, 99: 1-30.

Onchoke, Kefa K. 2021. '13C NMR chemical shift assignments of nitrated benzo[a]pyrenes based on two-dimensional techniques and DFT/GIAO calculations', *Results in Chemistry*, 3: 100099.

Opiyo, George, and Jianyong Jin. 2021. 'Recent progress in switchable RAFT agents: Design, synthesis and application', *European Polymer Journal*, 159: 110713.

Rahman, Sharifur, Malik Abdul Rub, Shamim Mahbub, Md Tuhinur R. Joy, Shahed Rana, and Md Anamul Hoque. 2022. 'Spectroscopic and DFT studies of the charge transfer complexation of iodine with aniline and its derivatives in carbon tetrachloride medium', *Journal of Molecular Liquids*, 351: 118667.

Sert, Yusuf, Sanae Lahmidi, Mohamed El Hafi, Halil Gökce, El Mokhtar Essassi, Abdelaziz Ejjoumamany, and Joel T. Mague. 2020. 'Spectral, DFT/B3LYP and molecular docking analyses on ethyl 2-(5-methyl-1,2,4-triazolo[1,5-a]pyrimidin-7-yl)pent-4-enoate', *Journal of Molecular Structure*, 1206: 127680.

Sherin, D. R., and T. K. Manojkumar. 2020. 'Significance of five membered heterocycles in fine tuning of HOMO-LUMO gap of simple donor-acceptor system as organic solar cell material: A DFT approach', *Materials Today: Proceedings*, 33: 1229-33.

Shukla, Bindesh Kumar, and Umesh Yadava. 2022. 'DFT calculations on molecular structure, MEP and HOMO-LUMO study of 3-phenyl-1-(methyl-sulfonyl)-1H-pyrazolo[3,4-d]pyrimidine-4-amine', *Materials Today: Proceedings*, 49: 3056-60.

Solğun, Derya Güngördü, Mehmet Salih Keskin, Ümit yıldıko, and Mehmet Salih Ağırtaş. 2020. 'DFT analysis and electronic properties, and synthesis of tetra (9-phenyl-9H-xanthen-9-yl) oxy peripheral-substituted zinc phthalocyanine', *Chemical Papers*, 74: 2389-401.

Solğun, Derya Güngördü, Ümit Yıldıko, and Mehmet Salih Ağırtaş. 2021. 'Synthesis, DFT Calculations, Photophysical, Photochemical Properties of Peripherally Metallophthalocyanines Bearing (2-(Benzo[d] [1,3] Dioxol-5-Ylmethoxy) Phenoxy) Substituents', *Polycyclic Aromatic Compounds*: 1-19.

Sucheta, M., A. G. Pramod, Mohamed Zikriya, K. Mohammed Salma, N. Venugopal, R. Chaithra, D. Harshitha, S. Amudan, C. G. Renuka, and Shiva Murthy. 2022. 'Frontier molecular orbital, molecular structure and Thermal properties of 2,4,6,8-tetramethyl-2,3,6,7-tetrahydro-s-indacene-1,5-dione using DFT calculation', *Materials Today: Proceedings*.

Tarchouna, S., I. Chaabane, and A. Ben Rahaiem. 2016. 'FT-IR and Raman spectra and vibrational investigation of bis (4-acetylanilinium) hexachlorostannate using DFT (B3LYP) calculation', *Physica E: Low-dimensional Systems and Nanostructures*, 83: 186-94.

Yildiko, Umit, Ahmet Çağri Ata, Aslihan Aycan Tanriverdİ, and İsmaİl Çakmak. 2021. 'Investigation of novel diethanolamine dithiocarbamate agent for RAFT polymerization: DFT computational study of the oligomer molecules', *Bulletin of Materials Science*, 44: 186.

Yildiko, Ümit, Ahmet Cagri Ata, and İsmail Cakmak. 2020. 'Synthesis, spectral characterization and DFT calculations of novel macro MADIX agent: mechanism of addition-fragmentation reaction of xanthate compound', *SN Applied Sciences*, 2: 1691.

Zahedi, Hamid, and Nahid Farzi. 2022. 'The simulation of a green room-temperature ternary solution of water, methanol and 1-ethyl-3-methyl imidazolium chloride by all-atom Monte Carlo and DFT computational approaches', *Journal of Molecular Liquids*, 356: 118903.